

1 **The embryonic node functions as an instructive stem cell niche**

2

3 **Authors:** Tatiana Solovieva¹, Hui-Chun Lu¹, Adam Moverley^{1,2}, Nicolas Plachta² and Claudio
4 D. Stern^{1*}

5 **Affiliations:**

6 ¹ Department of Cell and Developmental Biology, University College London

7 ² Institute of Molecular Cell Biology, A*STAR, Singapore

8 *Corresponding author. E-mail: c.stern@ucl.ac.uk

9

10 **In warm-blooded vertebrate embryos (mammals and birds), the body forms from a**
11 **growth zone at the tail end. Hensen's node, a region which induces and patterns the**
12 **neural axis is located within this growth zone. The node also contains the precursors of**
13 **neural, mesodermal and endodermal structures along the midline and has been suggested**
14 **to contain a small population of resident stem cells. However, it is unknown whether the**
15 **rest of the node constitutes an instructive stem cell niche, specifying stem cell behaviour.**
16 **Here we combine transplantation of a single cell in vivo with single-cell mRNA sequencing**
17 **in the chick and show that when made to enter the node, non-node-progenitor cells**
18 **become resident and gain stem cell behaviour. These cells preferentially express G2/M**
19 **phase cell-cycle related genes and are concentrated in posterior sub-regions of the node.**
20 **The posterior part of the node therefore behaves as an instructive stem cell niche. These**
21 **results demonstrate a new function for the vertebrate node during development.**

22

23 In higher vertebrate embryos, the body axis forms in head-to-tail direction from a growth zone
24 at the tail end which is present from gastrula stages through to the end of axis elongation.
25 During gastrulation (in chick: stage HH3+ to HH4)¹, epiblast cells lateral to the anterior tip of
26 the streak/node ingress into it. After this, the node begins to regress caudally² as cells exit the
27 node to lay down the midline of the developing head-tail axis (Fig. 1 a-c)³⁻⁶. However,
28 transplantation of cell groups and fate mapping experiments in chick^{4,7-9} and mouse¹⁰⁻¹⁴ during
29 early development have suggested that the node contains some resident, self-renewing cells
30 that persist during axial elongation in the node, while other cells leave (Fig. 1c, ‘RC’). Could
31 the former be stem cells¹⁵, specified by neighbouring node cells?

32

33 There are two possibilities: either there is a special population of stem cells set aside during
34 early development that is maintained by the node environment (“permissive”), or the node
35 constitutes a special niche that can instruct any cell to acquire self-renewing stem cell
36 characteristics¹⁶⁻¹⁸. To demonstrate self-renewal and to test whether the node is an instructive
37 stem cell niche, it is critical to challenge the responses of an individual cell to the node
38 environment. Here we use transplantation of single cells *in vivo* and single-cell RNA
39 sequencing (scRNA-seq) to describe a cell’s response to the node.

40

41 **Non-node cells can become resident**

42 To test whether the node environment can impart resident behaviour onto other cells, we
43 grafted anterior epiblast (which never normally enters the node^{5,19-21}) to a position adjacent to
44 the HH3+/4 node, so that transplanted cells would be carried into the node by gastrulation
45 movements (Fig. 1f). Graft-derived cells (from the transgenic GFP-donor) give rise to axial
46 tissues and express appropriate molecular markers of node, notochord and somite (Fig. 1g,

47 Extended Data Fig. 1a-j). Importantly, the contribution of this anterior epiblast to cells with
48 resident behaviour (88%, n=30/34) is similar to that of lateral epiblast (Fig1. d-e, Extended
49 Data Fig. 1k) (89%, n=8/9), which does normally enter the node. These results show that the
50 node can confer resident behaviour and axial identity.

51

52 **Prospective node cells are plastic**

53 To test whether cells are intrinsically committed to node and axial identities, we prevented
54 lateral epiblast cells from entering the node by grafting them into a remote anterior position
55 (Fig. 1j). After culture to HH8-10, graft-derived cells localize to and resemble head structures
56 rather than node derived tissues and fail to express the node marker, chordin (Fig. 1k). Lateral
57 cells therefore develop according to their new anterior position^{5,19-21} (Fig. 1h-i), demonstrating
58 that cells normally destined to give rise to node and axial identities are not committed to these
59 before they enter the node.

60

61 **Self-renewal specified by a node niche**

62 We then asked whether resident cells specified by the node are stem cells by testing for self-
63 renewal, a key characteristic of a stem cell²²⁻²⁴. First, anterior epiblast was made to enter the
64 node by grafting adjacent to it at HH3+/4 (Extended Data Fig. 2a-b). Following culture to HH8-
65 10, two to ten GFP-positive cells remaining in the node were re-grafted into a second, younger
66 (HH3+/4) host node (Extended Data Fig. 2c-f) to determine whether the GFP-positive cells can
67 self-renew and contribute daughters to the developing axis for a second time. GFP-positive
68 cells contributed to both node and axis in 17% of embryos (n=4/23) (Extended Data Fig. 2g-i)
69 suggesting self-renewal.

70

71 To demonstrate this at the single-cell level we repeated the re-grafts (again using two
72 successive hosts) with just a single GFP-positive resident cell (Fig. 2). After culture of the
73 second host to HH8-10 (Fig. 2e-f), GFP-positive cells were detected in 21% of grafted embryos
74 (n=11/53) (Extended Data Fig. 2j), of which 36% had multiple GFP-positive cells, showing
75 that cell division had occurred; 18% had GFP-positive cells in both node and axis revealing
76 that the resident cells both self-renewed and contributed to the axial midline (Fig. 2f-g). The
77 node's ability to specify self-renewing resident behaviour from cells not normally destined to
78 enter it clearly demonstrates the properties of an instructive niche¹⁶⁻¹⁸.

79

80 To test whether this niche relies on neighbouring supporting cells, re-grafts of an individual
81 GFP-positive cell were performed alone (n=26), or attached to a few neighbouring GFP-
82 negative cells from the first host (n=27). While survival and division of GFP-positive cells was
83 comparable between these two conditions, GFP-positive cells attached to GFP-negative
84 neighbours showed an increased contribution to the node when compared to GFP-positive cells
85 grafted alone (40% versus 17%) (Extended Data Fig. 2j). This finding is also consistent with
86 the idea that the node behaves like an instructive niche, inducing self-renewal behaviour on
87 other cells.

88

89 **Properties of node sub-regions**

90 Does the entire node act as a niche, or is this property located in a particular sub-region? To
91 identify the regions containing long-term resident cells, we constructed a fate map of the node
92 by labelling each of six sub-regions using a lipophilic dye (DiI) at HH8 (Extended Data Fig.
93 3a). After culture to HH11-12, all cells from anterior sub-regions had come out from the node
94 and the middle sub-regions contributed to anterior parts of the later node (chordoneural hinge),
95 while only the posterior sub-regions continued to contribute to the entire older node and its

96 derivatives (Fig. 3a-b, Extended Data Fig. 3b-g). This suggests that resident cells remaining in
97 the node the longest are confined to posterior sub-regions. Consistent with this, in the re-
98 grafting experiments described earlier, the single cell remaining in the node was always found
99 in the posterior sub-region (Fig. 2f-g). Furthermore, live imaging of embryos in which a mosaic
100 of cells was fluorescently-labelled revealed endogenous resident cells remaining in the
101 posterior node as it regresses (HH5-9), whereas most cells from other regions of the node were
102 left behind to contribute to the axis (Supplementary Movie 1). This is consistent with fate
103 mapping results of the mouse node, showing that some labelled cells remain in the node-
104 primitive-streak border as the axis forms^{14,25}. The posterior node is therefore the strongest
105 candidate for an axial stem cell niche in amniotes. This is further supported by findings that
106 when the posterior part of the node is removed, axial elongation is impaired^{9,25}.

107

108 **Molecular properties of resident cells**

109 What are the molecular characteristics of cells residing in this posterior niche? We grafted
110 GFP-epiblast from next to the node to the same position in a wild-type host and cultured the
111 embryos to HH8. Single graft-derived cells were collected from the posterior, middle and
112 anterior regions of the HH8 node, and processed for scRNA-seq using SmartSeq (Fig. 3c). The
113 data were examined by Principal Component (PC) analysis (Extended Data Fig. 5a); the first
114 component (PC1) groups cells into two clusters, one composed largely of posterior cells (Fig.
115 3d). To identify the genes causing this clustering, we calculated the correlation coefficient of
116 genes for PC1. Thirty-seven genes have significant expression in the posterior cluster
117 (correlation coefficient <-0.8); the majority of these (31/37) encode proteins of the G2/M
118 phases of the cell cycle (Fig. 3e-f, Extended Data Fig. 4). This suggests that these cells are
119 preparing to divide. Graft-derived cells isolated from other parts of the node appear to be
120 randomly distributed in other phases of the cell cycle (Extended Data Fig. 5b-f).

121

122 To determine whether the posterior region of the node is a unique site for cells at the G2/M
123 phases of the cycle, we compared the transcriptomes of entire node sub-regions at HH8
124 (Extended Data Fig. 7a). Half of the cell-cycle related genes identified in the scRNA-seq were
125 also enriched in the posterior node as a whole, while the other half, including CDK1, were
126 instead enriched in anterior regions (Fig. 3f versus 3g, Extended Data Fig. 6). Expression of
127 these G2/M cell-cycle related genes is therefore specific to individual resident cells, but not
128 necessarily to their micro-environment. This suggests that dividing resident cells may make up
129 only a small proportion of the node niche. Interestingly, the transcriptomes of the sub-regions
130 reveal an enrichment of genes involved in Wnt, Notch and FGF signalling in the posterior part
131 of the node (Extended Data Fig. 7). These three pathways have been implicated in other stem
132 cell niches¹⁸.

133

134 **Competence to respond to the node niche**

135 If anterior epiblast cells can acquire resident, self-renewing behaviour in response to the node
136 environment, can any epiblast cell be similarly induced? To answer this, epiblast from older
137 stage embryos (HH4+/5, corresponding to prospective neural plate) was used as donor tissue
138 (Fig. 4a-b)^{3,26}. This later HH4+/5 epiblast was forced to enter a younger (HH3+/4) node by
139 grafting just adjacent to it (Fig. 4c-e). After culture to HH8-11, graft-derived cells from these
140 late-to-early transplants contributed to the same axial and paraxial structures as the grafts from
141 younger donors described earlier (Extended Data Fig. 8a). However, late epiblast gave rise to
142 caudal node and/or chordoneural hinge in fewer embryos (55%) than lateral or anterior epiblast
143 (89% and 88% respectively) suggesting that late epiblast cells are less able to respond to the
144 node environment. Late epiblast cells also give rise to mesodermal structures (notochord and
145 PSM/medial somite) less frequently than either lateral or anterior epiblast, and some that do,

146 fail to express appropriate mesodermal genes (Fig. 4e). In contrast, late grafts contribute more
147 frequently to neural structures (floorplate, 45% and lateral neural plate, 27%) than younger
148 lateral epiblast (33% and 11% respectively) (Extended Data Fig. 8a). At the time of grafting,
149 donor late epiblast cells already express neural plate markers (including SOX2 and ZEB2)
150 (Extended Data Fig. 8b-g), but following grafting they lose expression of these genes except
151 for descendants contributing to neural structures (Extended Data Fig. 8h-k). This suggests that
152 the node environment causes late epiblast cells to lose their neural plate identity but is not
153 sufficient to convert them fully into axial mesoderm. This transition away from mesodermal
154 and towards neural fates appears to take place around stages HH5- to HH5 (Extended Data Fig.
155 8l) and suggests that older, neural plate epiblast has lost its competence to respond to signals
156 from the node niche that induce axial identity and resident behaviour.

157

158 What molecular changes underlie this loss of competence? To address this we performed
159 scRNA-seq on cells with resident behaviour at HH8, originating from non-competent cells
160 (from late-to-early grafts) and compared these to cells that are competent (from grafts of lateral
161 or anterior epiblast) (Extended Data Fig. 9a-c). Irrespective of origin, the most significant
162 variation among the cells could still be accounted for by their expression of G2/M-phase related
163 cell-cycle genes (Extended Data Fig. 9d-g, compare with Fig. 3d-e; clustering by PC1-2).
164 However, PC3-4 clusters cells into overlapping groups according to their donor origin (lateral,
165 anterior or late epiblast) (Fig. 4f). A subset of late-epiblast-derived cells that is associated with
166 limited competence is characterised by specific expression of 15 genes (correlation coefficient
167 >0.55 with PC3) (Extended Data Fig. 10a). Of these genes, seven have known roles in cell
168 adhesion and/or in neural development including NCAM1 and CLDN1, normally expressed
169 mainly in the neural plate (Fig. 4g-i and Extended Data Fig. 10b-i). This suggests that these

170 later cells may have lost their competence to respond to the node environment because they
171 have already initiated their differentiation into neural plate.

172

173 **Conclusion**

174 Until now, apart from a few studies using prospective single cell fate mapping^{4,10,11}, evidence
175 for resident cells in the node was based on studies of cell populations^{8,9,12-14}. Without
176 challenging behaviour at the single cell level it has not been possible to test whether the node
177 represents an instructive stem cell niche. Here, using single cell grafts we discovered that the
178 node can specify resident and self-renewing behaviour. Thus, in addition to its well-known
179 roles as an ‘organizer’ of the amniote embryo²⁷⁻²⁹ and its ability to dorsalize mesoderm^{30,31},
180 this key embryonic structure also functions as a stem cell niche that can specify resident stem
181 cells for the developing head-tail axis.

182

183 **Main references**

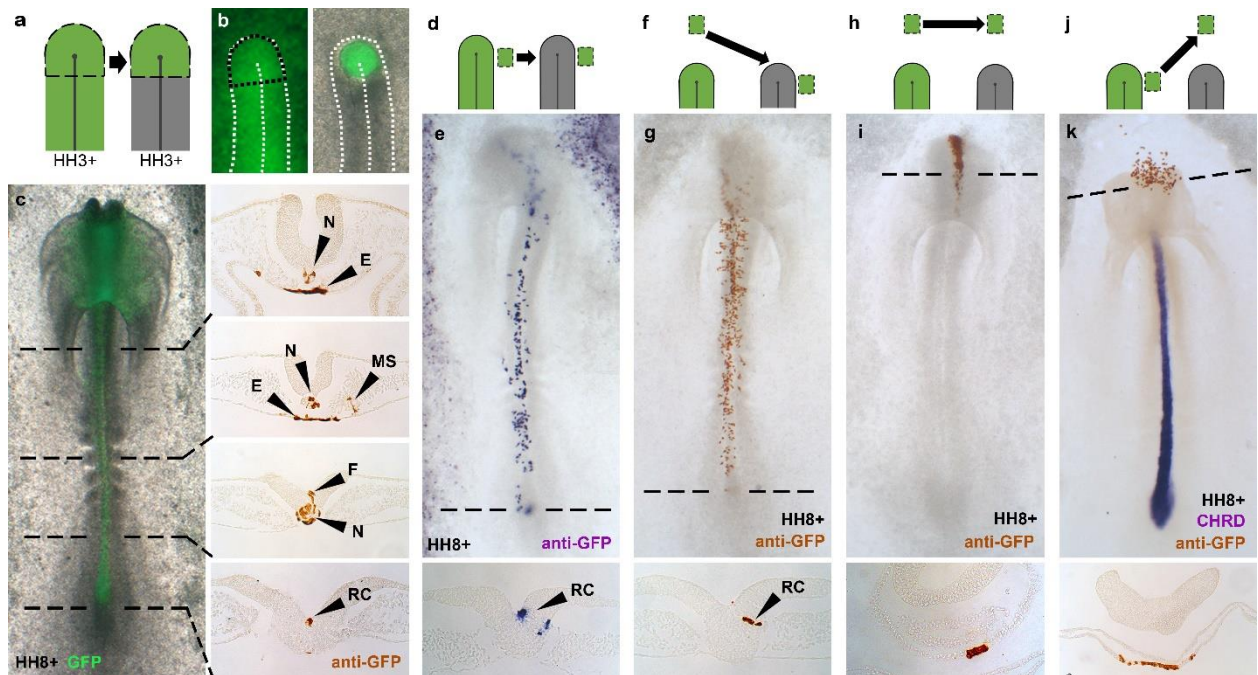
- 184 1 Hamburger, V. & Hamilton, H. L. A series of normal stages in the development of the
185 chick embryo. *J. Morphol.* **88**, 49-92 (1951).
- 186 2 Spratt, N. T. Regression and shortening of the primitive streak in the explanted chick
187 blastoderm. *J. Exp. Zool.* **104**, 69-100 (1947).
- 188 3 Joubin, K. & Stern, C. D. Molecular interactions continuously define the organizer
189 during the cell movements of gastrulation. *Cell* **98**, 559-571 (1999).
- 190 4 Selleck, M. & Stern, C. D. Fate mapping and cell lineage analysis of Hensen's node in
191 the chick embryo. *Development* **112**, 615-626 (1991).
- 192 5 Rosenquist, G. C. A radio autographic study of labelled grafts in the chick blastoderm
193 development from primitive streak stages to stage 12. *Contr. Embryol. Cameg. Inst.*
194 *Washington* **38**, 71-110 (1966).

- 195 6 Rosenquist, G. C. The chorda center in Hensen's node of the chick embryo. *The*
196 *Anatomical Record* **207**, 349-355 (1983).
- 197 7 Mathis, L., Kulesa, P. M. & Fraser, S. E. FGF receptor signalling is required to
198 maintain neural progenitors during Hensen's node progression. *Nat. Cell Biol.* **3**, 559
199 (2001).
- 200 8 McGrew, M. J. *et al.* Localised axial progenitor cell populations in the avian tail bud
201 are not committed to a posterior Hox identity. *Development* **135**, 2289-2299 (2008).
- 202 9 Charrier, J.-B., Teillet, M.-A., Lapointe, F. & Le Douarin, N. M. Defining subregions
203 of Hensen's node essential for caudalward movement, midline development and cell
204 survival. *Development* **126**, 4771-4783 (1999).
- 205 10 Lawson, K. A., Meneses, J. J. & Pedersen, R. Clonal analysis of epiblast fate during
206 germ layer formation in the mouse embryo. *Development* **113**, 891-911 (1991).
- 207 11 Forlani, S., Lawson, K. A. & Deschamps, J. Acquisition of Hox codes during
208 gastrulation and axial elongation in the mouse embryo. *Development* **130**, 3807-3819
209 (2003).
- 210 12 Tam, P. & Tan, S.-S. The somitogenetic potential of cells in the primitive streak and
211 the tail bud of the organogenesis-stage mouse embryo. *Development* **115**, 703-715
212 (1992).
- 213 13 Cambray, N. & Wilson, V. Axial progenitors with extensive potency are localised to
214 the mouse chordoneural hinge. *Development* **129**, 4855-4866 (2002).
- 215 14 Cambray, N. & Wilson, V. Two distinct sources for a population of maturing axial
216 progenitors. *Development* **134**, 2829-2840 (2007).
- 217 15 Selleck, M. A. & Stern, C. D. in *Formation and differentiation of early embryonic*
218 *mesoderm* Ch. Evidence for stem cells in the mesoderm of Hensen's node and their
219 role in embryonic pattern formation, 23-31 (Springer, 1992).

- 220 16 Schofield, R. The relationship between the spleen colony-forming cell and the
221 haemopoietic stem cell. *Blood Cells* **4**, 7-25 (1978).
- 222 17 Dexter, T. M., Allen, T. D. & Lajtha, L. Conditions controlling the proliferation of
223 haemopoietic stem cells in vitro. *J. Cell. Physiol.* **91**, 335-344 (1977).
- 224 18 Li, L. & Xie, T. Stem cell niche: structure and function. *Annu. Rev. Cell Dev. Biol.* **21**,
225 605-631 (2005).
- 226 19 Spratt, N. T. Localization of the prospective neural plate in the early chick
227 blastoderm. *J. Exp. Zool.* **120**, 109-130 (1952).
- 228 20 Bortier, H. & Vakaet, L. Fate mapping the neural plate and the intraembryonic
229 mesoblast in the upper layer of the chicken blastoderm with xenografting and time-
230 lapse videography. *Development* **116**, 93-97 (1992).
- 231 21 Hatada, Y. & Stern, C. D. A fate map of the epiblast of the early chick embryo.
232 *Development* **120**, 2879-2889 (1994).
- 233 22 Becker, A. J., McCulloch, E. A. & Till, J. E. Cytological demonstration of the clonal
234 nature of spleen colonies derived from transplanted mouse marrow cells. *Nature*, **197**,
235 452-454 (1963).
- 236 23 Siminovitch, L., McCulloch, E. A. & Till, J. E. The distribution of colony-forming
237 cells among spleen colonies. *J. Cell. Comp. Physiol.* **62**, 327-336 (1963).
- 238 24 Till, J. E., McCulloch, E. A. & Siminovitch, L. A stochastic model of stem cell
239 proliferation, based on the growth of spleen colony-forming cells. *Proc. Natl. Acad.*
240 *Sci. U. S. A.* **51**, 29 (1964).
- 241 25 Wymeersch, F. J. *et al.* Transcriptionally dynamic progenitor populations organised
242 around a stable niche drive axial patterning. *Development* **146**, dev168161 (2019).

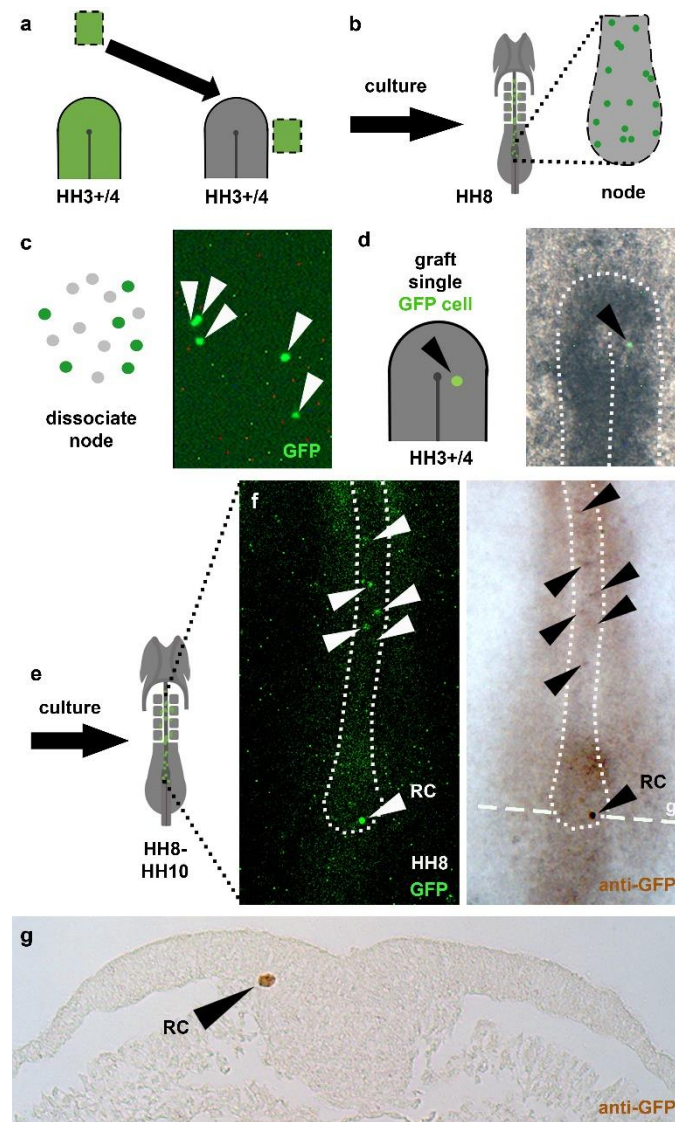
- 243 26 Sheng, G., dos Reis, M. & Stern, C. D. Churchill, a zinc finger transcriptional
244 activator, regulates the transition between gastrulation and neurulation. *Cell* **115**, 603-
245 613 (2003).
- 246 27 Waddington, C. Developmental mechanics of chicken and duck embryos. *Nature* **125**,
247 924 (1930).
- 248 28 Waddington, C. Experiments on determination in the rabbit embryo. *Arch. Biol* **48**,
249 273-290 (1937).
- 250 29 Anderson, C. & Stern, C. D. Organizers in development. *Curr. Top. Dev. Biol.* **117**,
251 435-454 (2016).
- 252 30 Streit, A. & Stern, C. D. Mesoderm patterning and somite formation during node
253 regression: differential effects of chordin and noggin. *Mech. Dev.* **85**, 85-96 (1999).
- 254 31 Nicolet, G. Is the presumptive notochord responsible for somite genesis in the chick?
255 *Development* **24**, 467-478 (1970).
- 256
- 257
- 258

259



260

261 **Figure 1 | The node confers resident behaviour and axial fates.** a-c, Node replacement using
 262 a GFP-donor showing normal node axial fates. d-e, Epiblast lateral to the HH3+/4 node
 263 ingresses into it and gives rise to the axis and to regressor node as 'resident cells' (RC). f-g,
 264 Anterior epiblast not normally fated to enter the node behaves as lateral epiblast when forced
 265 to do so. h-i, Anterior epiblast normally gives rise to head structures. j-k, Lateral epiblast no
 266 longer gives rise to node-derived axial structures when prevented from entering the node.
 267 N=notochord; E=endoderm; MS=medial-somite; F=floorplate; RC=resident cell. Transverse
 268 dashed lines show levels of accompanying sections.



269

270 **Figure 2 | Single cell re-grafts reveal that the node can specify self-renewing resident cells.**

271 **a**, Anterior epiblast not normally fated to enter the node was made to do so. **a-c**, After culture,

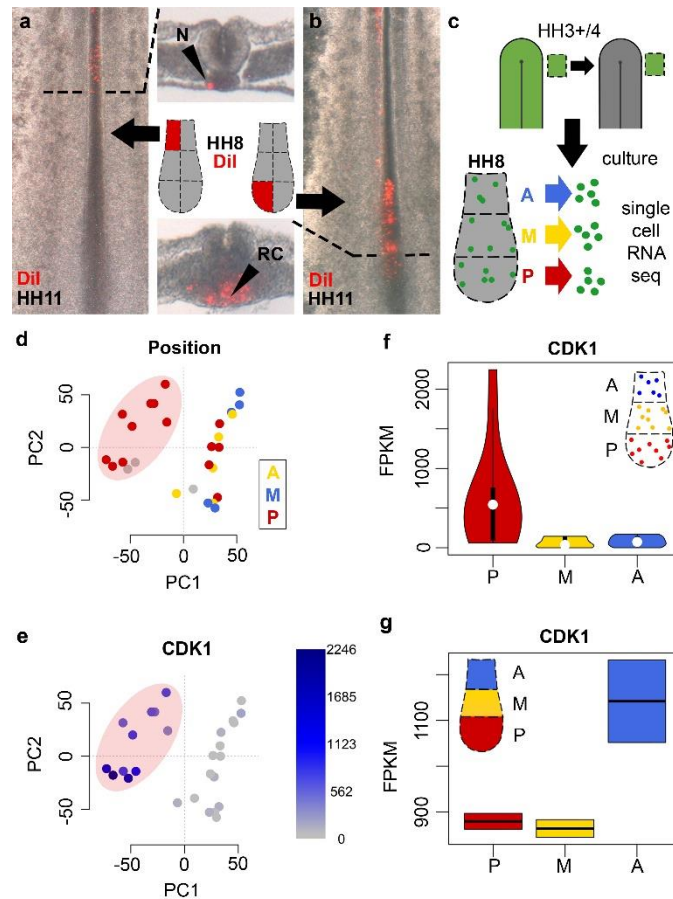
272 cells still residing in the HH8 node (b) were dissociated (c). **d**, A single GFP-positive cell was

273 isolated and grafted into a second younger, HH3+/4 host node. **e-g**, After culture (e), the single

274 GFP-positive cell had proliferated and descendants were found resident in the node and along

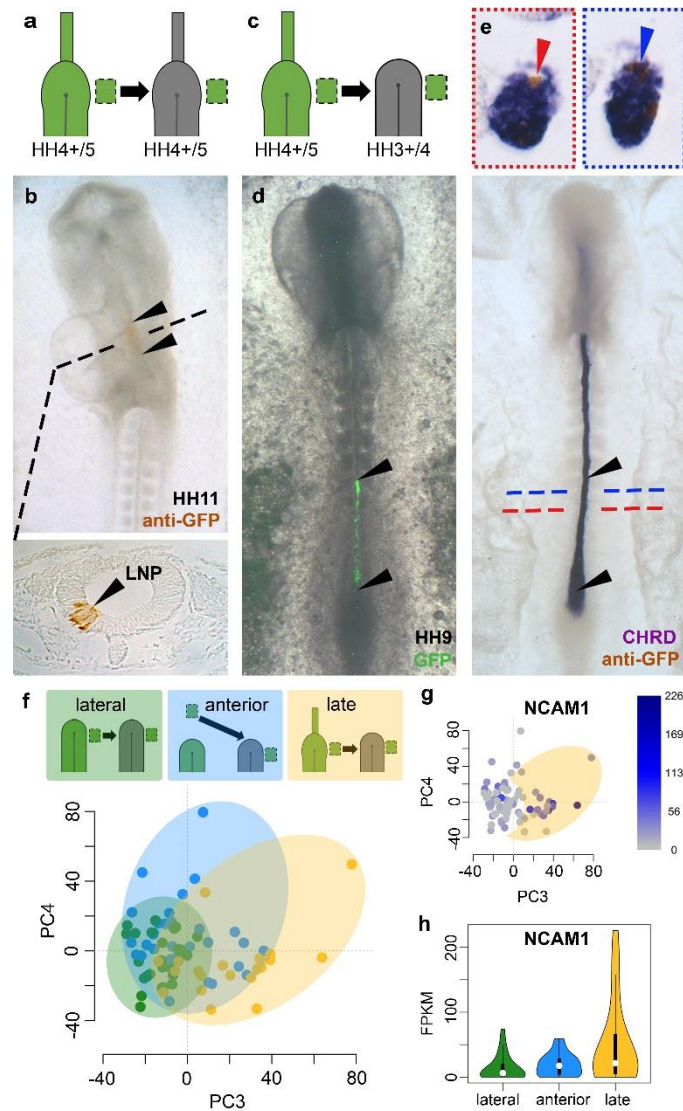
275 the axis (f-g). Transverse dashed line in (f) shows level of section in (g). RC=resident cell.

276



277

278 **Figure 3 | Long-term resident cells reside in the posterior node and are enriched in G2/M-**
 279 **phase cell-cycle genes. a-b,** Fate mapping of six domains reveals that only posterior sub-
 280 regions continue to contribute to resident cells. **c,** Individual resident cells originating from
 281 lateral epiblast were isolated from anterior (blue), middle (yellow) and posterior (red) HH8
 282 node sub-regions and processed for scRNA-seq. **d-e,** PC analysis reveals a cluster of posterior
 283 cells (pink oval) (d) enriched in G2/M-phase-related genes, including CDK1 (e) (intensity of
 284 blue reflects FPKM levels). **f-g,** While single posterior resident cells are enriched in CDK1 (f),
 285 bulk-RNA-seq shows that this is not the case in all cells of that region.



286

287 **Figure 4: Older epiblast is not competent to respond to the node. a-b,** ('Late') epiblast
 288 lateral to the HH4+/5 node normally contributes to lateral neural plate (LNP). **c-e,** When made
 289 to enter the younger node (c), 'late' epiblast contributes to the axial midline (d-e). Black
 290 arrowheads show the extent of head-to-tail contribution. While some graft-derived cells
 291 (visualised by anti-GFP) in the notochord express the notochord marker CHRDR (blue arrow),
 292 others do not (red arrow). **f-h,** Single cells from the HH8 node plotted using PC3/4 cluster
 293 according to their epiblast origin (lateral, anterior or late) (f). Expression of neural plate-like
 294 genes, including NCAM1, correlates with 'late' cells outside of the control (green) cluster
 295 (yellow oval) (g-h). Intensity of blue in (g) reflects FPKM levels.

296 **Methods**

297 **Embryos:** Wild type chicken embryos were obtained from Brown Bovan Gold hens (Henry
298 Stewart Farm). Transgenic cytoplasmic GFP chicken embryos were supplied by the avian
299 transgenic facility at The Roslin Institute, Edinburgh⁸. All eggs were incubated at 38°C in
300 humidified incubators and staged according to Hamburger and Hamilton¹. For grafting
301 experiments, *ex-ovo* embryo cultures were prepared using the New technique³² with
302 modifications as described by Stern and Ireland³³.

303

304 **Epiblast grafts:** Donor embryos were isolated in Tyrode's solution³⁴. The donor embryo was
305 turned ventral side up, underlying endodermal and mesodermal layers were peeled away and a
306 piece of epiblast (~20-50 cells) was cut out using 30G syringe needles. The epiblast piece was
307 checked to ensure no mesodermal/endodermal cells remained. An equal sized piece of epiblast
308 was removed from the host in the desired location and replaced with the donor epiblast. For
309 'lateral-to-lateral' grafts (see Fig. 1d), epiblast was grafted into the equivalent position in the
310 host as its donor origin (i.e. 'left-to-left' or 'right-to-right'). The 'lateral epiblast' was taken
311 from immediately adjacent to the tip of the streak/node. 'Anterior' epiblast was taken from a
312 midline position, about half-way between the tip of the streak/node and the anterior area opaca.

313

314 **Re-grafts of groups of cells:** The first graft was an epiblast graft from a GFP-donor to a non-
315 GFP host (see Extended Data Fig. 2a-b). The second graft (re-graft) included a group of cells
316 from the first host's node, containing 2-10 GFP-positive cells alongside some neighbouring
317 GFP-negative cells. A small 'nick' was made in the node (ventral side) of the second host into
318 which this group of cells was inserted using 30G syringe needles to carefully manoeuvre the
319 small pieces of tissue (see Extended Data Fig. 2c-f). The grafted embryos were left at room

320 temperature for ~15 min to aid attachment of the graft to the host before further incubation.

321 Embryos were cultured to HH8-10.

322

323 **Single cell re-grafts:** The first host had an ‘anterior-to-lateral’ graft (see Fig. 2a). After culture
324 to HH8-10, a single GFP-positive cell was collected from the host node (see ‘single cell
325 manipulation’ below) and then transferred using a micropipette made from a pulled 50 μ l
326 calibrated micropipette (Drummond Scientific, Cat 2-000-050) attached to an aspirator tube,
327 into the second host (HH3+/4) (see Fig. 2b-d). For some re-grafts, a single GFP-positive cell
328 was transferred attached to one or more neighbouring GFP-negative cells from the first host
329 (but there was never more than one GFP-positive cell). A small ‘nick’ was made in the node
330 of the second host. The GFP-positive cell was maneuvered into this nick by gently ‘blowing’
331 saline on the cell with a micropipette. Ideally, once placed into its pocket, a flap of tissue would
332 be used to cover the transplant site. The grafted embryo was then left at room temperature for
333 ~15 min to aid attachment of the cell to the host. Each New culture was checked by
334 fluorescence microscopy again just prior to incubation to ensure that the grafted GFP-positive
335 cell was still in place. Embryos were cultured to HH8-10.

336

337 **DiI labelling:** The lipophilic dye, DiI (DiI-CellTracker CM, Molecular Probes Life
338 Technologies, # C7001) was used for fate mapping of the HH8 node. For 10 μ l of working
339 solution, 8.5 μ l of 0.3M sucrose and 1 μ l of 1:20,000 Tween-20 were used with 0.5 μ l of 2mM
340 DiI (in dimethylformamide). All components were first pre-heated at 65°C, thoroughly mixed
341 and dissolved. The protocol for preparation and application of DiI was adapted from^{4,35,36}. The
342 embryo was first prepared for New culture³² and kept submerged in Tyrode’s. The node sub-
343 region to be labelled was cut out using 30G syringe needles and transferred to a drop of

344 Tyrode's containing DiI (~9:1 Tyrode's : DiI working solution) and kept in the dark for 1-2
345 min. The tissue piece was then removed and washed in successive drops of Tyrode's to remove
346 any excess DiI before verifying that sufficient labelling had taken place, by fluorescence
347 microscopy. The tissue piece was replaced into its original position, preserving the original
348 dorsoventral orientation. Labelled embryos were cultured to ~HH11-12. After culture, embryos
349 were fixed in 4% paraformaldehyde in PBS for at least 4 days at 4°C. To assess the location of
350 the descendants of the DiI-labelled cells, several thick transverse sections were cut from each
351 embryo by hand, using a scalpel, with the embryo pinned securely using insect pins in a silicon
352 rubber-bottomed dish³⁴.

353

354 ***In situ* hybridization:** *in situ* hybridization with digoxigenin (DIG-)-labelled riboprobes was
355 carried out following established protocols³⁷⁻³⁹. Antisense DIG-riboprobes were synthesized
356 by restriction digest and *in vitro* transcription. Plasmids used: CHR⁴⁰, FOXA2^{41,42};
357 PARAXIS/TCF-15⁴³; ZEB2²⁶; SOX2⁴⁴; TBX6⁴⁵; DLL1⁴⁶; RSPO3 (ChEST784h18); NKAIN4
358 (ChEST110n2); DRAXIN (ChEST54511); CLDN1 (ChEST168n2); NCAM1 (ChEST845i20);
359 MSGN1 (ChEST90p23); CHST15 (ChEST391h17); AKAP12 (ChEST376j15); FOXM1
360 (ChEST313o15); TOP2A (ChEST849a2); NUF2 (ChEST450j22); CENPL (ChEST97i12);
361 MAD2L1BP (ChEST365n5).

362

363 **Immunohistochemistry:** anti-GFP antibody staining largely followed the methods described
364 by Stern³⁸ and Streit and Stern³⁹. Embryos were processed for anti-GFP antibody staining either
365 immediately after collection (and fixing in 4% PFA overnight at 4°C) or following *in situ*
366 hybridization.

367

368 **Histology:** Some embryos processed for *in situ* hybridization and/or anti-GFP antibody
369 staining were embedded in paraffin wax and sectioned using a microtome. Methods largely
370 followed those of Izpisúa-Belmonte et al.³⁷. All sections were transverse and 10 μ M thick.
371 Slides were mounted using a 3:1 solution of Canada balsam (Merck, # 1016910100) and
372 HistoClear (HS-202 HISTO-CLEAR II, National Diagnostics).

373

374 **Microphotography:** Images of all whole-mount embryos and thick sections were recorded
375 using transmitted light with an Olympus SZH10 stereomicroscope with epifluorescence optics.
376 Paraffin sections were examined on an Olympus Vanox-T optical microscope. A QImaging
377 Retiga 2000R Fast 1394 camera and QCapture Pro software was used for all image capture.

378

379 **Live imaging and cell tracking:** Electroporation mixture containing 1 mg.ml⁻¹ pDsRed-
380 Express plasmid, 6% (wt/vol) sucrose and 0.04% (wt/vol) Fast Green FCF was applied
381 dorsally, just lateral to the node of HH4- embryos to transfect ingressing cells. Electroporation
382 was performed in a custom-made chamber with four pulses of 5 V, 50 msec width, 500 ms
383 interval. Embryos were then cultured using a modification of New's method^{32,33} in 35 mm
384 plastic dishes with a glass coverslip base, and imaged with a Zeiss LSM 880 inverted
385 microscope using a Plan-Apochromat 20x, 0.8 NA objective. Images were acquired at 10 min
386 intervals using 3x5 tiling (10% overlap) to achieve coverage of the whole embryo. Image
387 analysis and cell tracking were performed using Imaris (Bitplane) software. The embryo was
388 imaged from the epiblast (dorsal) side but the output from Imaris is displayed as a mirror image
389 (pseudo-ventral view).

390

391 **Single cell manipulation:** For collection of single cells for single cell re-grafts and scRNA-
392 seq, the cultured embryo was first submerged in Tyrode's solution (for re-grafts) or sterile
393 molecular grade PBS with 0.1% glucose (for scRNA-seq). The node was then divided into
394 anterior, middle and posterior sub-regions of equal rostro-caudal length. Each of these regions
395 containing GFP-positive cells was cut out, in turn, and placed in a drop of non-enzymatic
396 dissociation medium (Sigma, # C5914-100ML), kept over ice. Each piece was washed twice
397 in drops (~30 μ l) of this dissociation medium while over ice. To help with dissociation, after
398 ~5 min, the tissue was gently aspirated up and down using a micropipette (made from a pulled
399 50 μ l calibrated micropipette (Drummond Scientific, Cat 2-000-050) attached to an aspirator
400 tube). The micropipette was broken at the tip to have a diameter just narrower than the width
401 of the tissue piece. Once the piece of tissue was fragmented, a capillary with a narrower tip
402 was used for further dissociation to single cells in suspension. GFP-positive cells were
403 identified by fluorescence under a dissection microscope (x70 magnification) and were
404 individually aspirated using a micropipette. The cell was transferred into a drop of Tyrode's
405 (for re-grafts) or of sterile molecular grade PBS (for scRNA-seq) to replace the dissociation
406 medium and to verify that there was only a single GFP-positive cell. Once verified, the cell
407 was transferred (using a fresh pulled micropipette) to the second host (for re-grafts) or into a
408 200 μ l tube containing 5 μ l of lysis buffer and 5% RNase inhibitor (for scRNA-seq) (lysis
409 buffer and RNase inhibitor from SMART-Seq v4 Ultra Low Input RNA Kit, Takara, # 634892).
410 Once the dissociation process began, cells were collected for ~20 min, after which time any
411 remaining dissociated tissue was discarded, and a new tissue piece taken from the embryo.

412

413 **scRNA-seq:** The SMART-Seq v4 Ultra Low Input RNA Kit (Takara, # 634892) targeting
414 mRNA, was used for preparing the single cells for sequencing. Amplified cDNA was purified
415 using AMPure magnetic purification beads (Agencourt AMPure XP, Beckman Coulter #

416 A63880). The DNA concentration of purified cDNA was checked by Qubit (dsDNA HS Assay
417 Kit, Thermofisher # Q33230). All samples yielding at least 5 ng of cDNA were sheared by
418 sonication (Covaris, S220/E220 focused-ultrasonicator, settings set to: 10% duty factor, 200
419 cycles per burst, 120 second treatment time, 175W peak incident power) to obtain ~500bp
420 fragments for library preparation. The ThruPLEX DNA-seq, Dual Index Kit (Takara, #
421 R400406) was used to construct dual indexed libraries for each sample. Libraries were
422 individually purified, using AMPure magnetic purification beads (Agencourt AMPure XP,
423 Beckman Coulter # A63880). DNA concentration of purified libraries was checked by Qubit
424 (dsDNA HS Assay Kit, Thermofisher # Q33230) and size distribution of cDNA measured
425 using TapeStation (Agilent High sensitivity D1000 screen tape, # 5067-5584). All libraries
426 were individually diluted to 10 nM in elution buffer before pooling together. Pooled libraries
427 were sequenced by UCL Genomics using an Illumina NextSeq sequencer with a 75bp single
428 end read cycle kit. The average number of reads per cell was ~10 Million (range: 6,838,400-
429 15,404,851). The single cell RNA-seq raw data have been deposited in EBI Array Express
430 (accession number E-MTAB-9116).

431

432 **RNA-seq of tissues:** Tissues (HH8 node sub-regions) were isolated from transgenic-GFP
433 embryos using 30G syringe needles in sterile molecular grade PBS. Tissues were collected into
434 RNAlater (Invitrogen, # AM7020). For each sample, tissues were collected from thirteen to
435 seventeen embryos. RNA was extracted using the Micro Total RNA Isolation Kit (Invitrogen,
436 # AM1931) and concentration and quality measured using TapeStation (Agilent High
437 sensitivity RNA screen tape, # 5067-5579). The NEBNext Single Cell/Low Input RNA Library
438 Prep Kit for Illumina (# E6420) was used for cDNA and library synthesis (performed by UCL
439 Genomics). Libraries were sequenced by Illumina NextSeq using a 75bp single end read cycle
440 kit. The average number of reads per sample (node sub-region) was ~22 Million (range:

441 19,572,310 to 24,523,360). The bulk RNA-seq raw data have been deposited in EBI Array
442 Express (accession number E-MTAB-9115).

443

444 **RNA-seq data processing:** Raw data were checked using FastQC⁴⁷ to assess overall quality.
445 Cutadapt⁴⁸ was used to remove low-quality bases (Phred quality score <20) at the 3' and 5'
446 ends, adapter sequences, primer sequences, and poly-A tails of each read. Reads were aligned
447 to the galGal6 chicken genome using TopHat2⁴⁹, alignment rates were 91.9%±0.3% (for
448 scRNA-seq) and 86.3%±0.65% (for RNA-seq of tissues). Transcripts were counted and
449 normalized using Cufflinks⁵⁰ programs *cuffquant* and *cuffnorm* respectively. Data analysis was
450 performed in the R environment (R-3.5.1).

451

452 For scRNA-seq, all sequenced cells passed quality control. The matrix of transcript FPKMs
453 (Fragments Per Kilobase of transcript per Million mapped reads) contains expression of 24,353
454 genes in 77 samples (cells). Of these, 13,817 are expressed (with an FPKM >0.5) in at least
455 two cells in our data. The top 5000 most variable of these genes were used for principal
456 component (PC) analysis. PC analysis was carried out on two datasets: data from single cells
457 from the HH8 node originating only from lateral epiblast (n=27) and data from single cells
458 from the HH8 node originating from anterior, lateral and late epiblast (n=77). Correlation
459 coefficients were calculated for the relationship between gene expression and a given principal
460 component.

461

462 For RNA-seq of tissues, all node sub-regions passed quality control. Mitochondrial RNAs,
463 ribosomal RNAs and microRNAs were excluded. Fold changes for each gene in posterior

464 sub-regions against its expression in all other regions were calculated to find genes with the
465 most marked differential expression between sub-regions (see Extended Data Fig. 7b).

466

467 **Data availability**

468 The scRNA-seq and bulk-RNA-seq raw datasets generated during the current study are
469 available in the EBI Array Express (<https://www.ebi.ac.uk/arrayexpress/>). Accession numbers:
470 E-MTAB-9116 and E-MTAB-9115.

471

472

473 **References for Methods and Extended Data**

474

- 475 32 New, D. A new technique for the cultivation of the chick embryo in vitro.
476 *Development* **3**, 326-331 (1955).
- 477 33 Stern, C. D. & Ireland, G. W. An integrated experimental study of endoderm
478 formation in avian embryos. *Anat. Embryol. (Berl.)* **163**, 245-263 (1981).
- 479 34 Stern, C. D. in *Essential Development Biology: A Practical Approach* (eds Claudio
480 D Stern & Peter WH Holland) Ch. Avian Embryos 45-54 (Oxford Univ. Press., 1993).
- 481 35 Psychoyos, D. & Stern, C. D. Fates and migratory routes of primitive streak cells in
482 the chick embryo. *Development* **122**, 1523-1534 (1996).
- 483 36 Ruiz i Altaba, A., Warga, R. M. & Stern, C. D. in *Essential developmental biology: a*
484 *practical approach* (eds Claudio D Stern & Peter WH Holland) Ch. Fate maps and
485 cell lineage analysis, 81-95 (Oxford Univ. Press 1993).

- 486 37 Izpisúa-Belmonte, J. C., De Robertis, E. M., Storey, K. G. & Stern, C. D. The
487 homeobox gene goosecoid and the origin of organizer cells in the early chick
488 blastoderm. *Cell* **74**, 645-659 (1993).
- 489 38 Stern, C. D. in *Cellular and molecular procedures in developmental biology* Vol. 36
490 *Current topics in developmental biology* (eds Flora de Pablo, Alberto Ferrus, &
491 Claudio D. Stern) Ch. Detection of multiple gene products simultaneously by in situ
492 hybridization and immunohistochemistry in whole mounts of avian embryos, 223-243
493 (Elsevier, 1998).
- 494 39 Streit, A. & Stern, C. D. Combined whole-mount in situ hybridization and
495 immunohistochemistry in avian embryos. *Methods* **23**, 339-344 (2001).
- 496 40 Streit, A. *et al.* Chordin regulates primitive streak development and the stability of
497 induced neural cells, but is not sufficient for neural induction in the chick embryo.
498 *Development* **125**, 507-519 (1998).
- 499 41 Levin, M., Johnson, R. L., Stern, C. D., Kuehn, M. & Tabin, C. A molecular pathway
500 determining left-right asymmetry in chick embryogenesis. *Cell* **82**, 803-814 (1995).
- 501 42 Nishizaki, Y., Shimazu, K., Kondoh, H. & Sasaki, H. Identification of essential
502 sequence motifs in the node/notochord enhancer of *Foxa2* (*Hnf3β*) gene that are
503 conserved across vertebrate species. *Mech. Dev.* **102**, 57-66 (2001).
- 504 43 Barnes, G. L., Alexander, P. G., Hsu, C. W., Mariani, B. D. & Tuan, R. S. Cloning
505 and Characterization of Chicken Paraxis: A Regulator of Paraxial Mesoderm
506 Development and Somite Formation. *Dev. Biol.* **189**, 95-111 (1997).
- 507 44 Uwanogho, D. *et al.* Embryonic expression of the chicken *Sox2*, *Sox3* and *Sox11*
508 genes suggests an interactive role in neuronal development. *Mech. Dev.* **49**, 23-36
509 (1995).

- 510 45 Knezevic, V., Santo De, R. & Mackem, S. Two novel chick T-box genes related to
511 mouse Brachyury are expressed in different, non-overlapping mesodermal domains
512 during gastrulation. *Development* **124**, 411-419 (1997).
- 513 46 Lee, H. C. *et al.* Molecular anatomy of the pre-primitive-streak chick embryo. *Open*
514 *biology* **10**, 190299 (2020).
- 515 47 Andrews, S. *FastQC: a quality control tool for high throughput sequence data*,
516 <<http://www.bioinformatics.babraham.ac.uk/projects/fastqc/>> (2010).
- 517 48 Martin, M. Cutadapt removes adapter sequences from high-throughput sequencing
518 reads. *EMBnet. journal* **17**, 10-12 (2011).
- 519 49 Kim, D. *et al.* TopHat2: accurate alignment of transcriptomes in the presence of
520 insertions, deletions and gene fusions. *Genome Biol.* **14**, R36 (2013).
- 521 50 Trapnell, C. *et al.* Differential analysis of gene regulation at transcript resolution with
522 RNA-seq. *Nat. Biotechnol.* **31**, 46 (2013).
- 523 51 Fang, L., Seki, A. & Fang, G. SKAP associates with kinetochores and promotes the
524 metaphase-to-anaphase transition. *Cell cycle* **8**, 2819-2827 (2009).
- 525 52 Sugata, N., Munekata, E. & Todokoro, K. Characterization of a novel kinetochore
526 protein, CENP-H. *J. Biol. Chem.* **274**, 27343-27346 (1999).
- 527 53 Sugata, N. *et al.* Human CENP-H multimers colocalize with CENP-A and CENP-C at
528 active centromere-kinetochore complexes. *Hum. Mol. Genet.* **9**, 2919-2926 (2000).
- 529 54 Li, F. *et al.* Control of apoptosis and mitotic spindle checkpoint by survivin. *Nature*
530 **396**, 580-584 (1998).
- 531 55 Hori, T., Haraguchi, T., Hiraoka, Y., Kimura, H. & Fukagawa, T. Dynamic behavior
532 of Nuf2-Hec1 complex that localizes to the centrosome and centromere and is
533 essential for mitotic progression in vertebrate cells. *J. Cell Sci.* **116**, 3347-3362
534 (2003).

- 535 56 Shaughnessy, J. Amplification and overexpression of CKS1B at chromosome band
536 1q21 is associated with reduced levels of p27 Kip1 and an aggressive clinical course
537 in multiple myeloma. *Hematology* **10**, 117-126 (2005).
- 538 57 Ayad, N. G. *et al.* Tome-1, a trigger of mitotic entry, is degraded during G1 via the
539 APC. *Cell* **113**, 101-113 (2003).
- 540 58 Gaitanos, T. N. *et al.* Stable kinetochore–microtubule interactions depend on the Ska
541 complex and its new component Ska3/C13Orf3. *The EMBO journal* **28**, 1442-1452
542 (2009).
- 543 59 Daum, J. R. *et al.* Ska3 is required for spindle checkpoint silencing and the
544 maintenance of chromosome cohesion in mitosis. *Curr. Biol.* **19**, 1467-1472 (2009).
- 545 60 Gaudet, S., Branton, D. & Lue, R. A. Characterization of PDZ-binding kinase, a
546 mitotic kinase. *Proceedings of the National Academy of Sciences* **97**, 5167-5172
547 (2000).
- 548 61 Matsumoto, S. *et al.* Characterization of a MAPKK-like protein kinase TOPK.
549 *Biochem. Biophys. Res. Commun.* **325**, 997-1004 (2004).
- 550 62 Lawo, S. *et al.* HAUS, the 8-subunit human Augmin complex, regulates centrosome
551 and spindle integrity. *Curr. Biol.* **19**, 816-826 (2009).
- 552 63 Einarson, M. B., Cukierman, E., Compton, D. A. & Golemis, E. A. Human enhancer
553 of invasion-cluster, a coiled-coil protein required for passage through mitosis. *Mol.*
554 *Cell. Biol.* **24**, 3957-3971 (2004).
- 555 64 Dunleavy, E. M. *et al.* HJURP is a cell-cycle-dependent maintenance and deposition
556 factor of CENP-A at centromeres. *Cell* **137**, 485-497 (2009).
- 557 65 Foltz, D. R. *et al.* Centromere-specific assembly of CENP-a nucleosomes is mediated
558 by HJURP. *Cell* **137**, 472-484 (2009).

- 559 66 Hori, T., Okada, M., Maenaka, K. & Fukagawa, T. CENP-O class proteins form a
560 stable complex and are required for proper kinetochore function. *Mol. Biol. Cell* **19**,
561 843-854 (2008).
- 562 67 Strunnikov, A. V., Hogan, E. & Koshland, D. SMC2, a *Saccharomyces cerevisiae*
563 gene essential for chromosome segregation and condensation, defines a subgroup
564 within the SMC family. *Genes Dev.* **9**, 587-599 (1995).
- 565 68 Hudson, D. F., Vagnarelli, P., Gassmann, R. & Earnshaw, W. C. Condensin is
566 required for nonhistone protein assembly and structural integrity of vertebrate mitotic
567 chromosomes. *Dev. Cell* **5**, 323-336 (2003).
- 568 69 Ono, T. *et al.* Differential contributions of condensin I and condensin II to mitotic
569 chromosome architecture in vertebrate cells. *Cell* **115**, 109-121 (2003).
- 570 70 Vanneste, D., Takagi, M., Imamoto, N. & Vernos, I. The role of Hklp2 in the
571 stabilization and maintenance of spindle bipolarity. *Curr. Biol.* **19**, 1712-1717 (2009).
- 572 71 Habu, T., Kim, S. H., Weinstein, J. & Matsumoto, T. Identification of a MAD2-
573 binding protein, CMT2, and its role in mitosis. *The EMBO journal* **21**, 6419-6428
574 (2002).
- 575 72 Xia, G. *et al.* Conformation-specific binding of p31comet antagonizes the function of
576 Mad2 in the spindle checkpoint. *The EMBO journal* **23**, 3133-3143 (2004).
- 577 73 Kimura, K., Cuvier, O. & Hirano, T. Chromosome Condensation by a Human
578 Condensin Complex in *Xenopus* Egg Extracts. *J. Biol. Chem.* **276**, 5417-5420 (2001).
- 579 74 Draetta, G. *et al.* Cdc2 protein kinase is complexed with both cyclin A and B:
580 evidence for proteolytic inactivation of MPF. *Cell* **56**, 829-838 (1989).
- 581 75 Dunphy, W. G., Brizuela, L., Beach, D. & Newport, J. The *Xenopus* cdc2 protein is a
582 component of MPF, a cytoplasmic regulator of mitosis. *Cell* **54**, 423-431 (1988).

- 583 76 Gautier, J., Norbury, C., Lohka, M., Nurse, P. & Maller, J. Purified maturation-
584 promoting factor contains the product of a *Xenopus* homolog of the fission yeast cell
585 cycle control gene *cdc2+*. *Cell* **54**, 433-439 (1988).
- 586 77 Fode, C., Binkert, C. & Dennis, J. W. Constitutive expression of murine Sak-a
587 suppresses cell growth and induces multinucleation. *Mol. Cell. Biol.* **16**, 4665-4672
588 (1996).
- 589 78 Habedanck, R., Stierhof, Y.-D., Wilkinson, C. J. & Nigg, E. A. The Polo kinase Plk4
590 functions in centriole duplication. *Nat. Cell Biol.* **7**, 1140-1146 (2005).
- 591 79 Earnshaw, W. C. & Rothfield, N. Identification of a family of human centromere
592 proteins using autoimmune sera from patients with scleroderma. *Chromosoma* **91**,
593 313-321 (1985).
- 594 80 Tomkiel, J., Cooke, C. A., Saitoh, H., Bernat, R. L. & Earnshaw, W. C. CENP-C is
595 required for maintaining proper kinetochore size and for a timely transition to
596 anaphase. *The Journal of cell biology* **125**, 531-545 (1994).
- 597 81 Korver, W., Roose, J. & Clevers, H. The winged-helix transcription factor Trident is
598 expressed in cycling cells. *Nucleic Acids Res.* **25**, 1715-1719 (1997).
- 599 82 Laoukili, J. *et al.* FoxM1 is required for execution of the mitotic programme and
600 chromosome stability. *Nat. Cell Biol.* **7**, 126 (2005).
- 601 83 Mills, G. B. *et al.* Expression of TTK, a novel human protein kinase, is associated
602 with cell proliferation. *J. Biol. Chem.* **267**, 16000-16006 (1992).
- 603 84 Schmandt, R., Hill, M., Amendola, A., Mills, G. B. & Hogg, D. IL-2-induced
604 expression of TTK, a serine, threonine, tyrosine kinase, correlates with cell cycle
605 progression. *The Journal of Immunology* **152**, 96-105 (1994).
- 606 85 Abrieu, A. *et al.* Mps1 is a kinetochore-associated kinase essential for the vertebrate
607 mitotic checkpoint. *Cell* **106**, 83-93 (2001).

- 608 86 Hogg, D. *et al.* Cell cycle dependent regulation of the protein kinase TTK. *Oncogene*
609 **9**, 89-96 (1994).
- 610 87 Sawin, K. E., LeGuellec, K., Philippe, M. & Mitchison, T. J. Mitotic spindle
611 organization by a plus-end-directed microtubule motor. *Nature* **359**, 540-543 (1992).
- 612 88 Wordeman, L. & Mitchison, T. J. Identification and partial characterization of mitotic
613 centromere-associated kinesin, a kinesin-related protein that associates with
614 centromeres during mitosis. *The Journal of cell biology* **128**, 95-104 (1995).
- 615 89 Okada, M. *et al.* The CENP-H-I complex is required for the efficient incorporation of
616 newly synthesized CENP-A into centromeres. *Nat. Cell Biol.* **8**, 446-457 (2006).
- 617 90 Mi, Y. *et al.* DEPDC1 is a novel cell cycle related gene that regulates mitotic
618 progression. *BMB reports* **48**, 413 (2015).
- 619 91 Hirose, K., Kawashima, T., Iwamoto, I., Nosaka, T. & Kitamura, T. MgcRacGAP is
620 involved in cytokinesis through associating with mitotic spindle and midbody. *J. Biol.*
621 *Chem.* **276**, 5821-5828 (2001).
- 622 92 DiNardo, S., Voelkel, K. & Sternglanz, R. DNA topoisomerase II mutant of
623 *Saccharomyces cerevisiae*: topoisomerase II is required for segregation of daughter
624 molecules at the termination of DNA replication. *Proceedings of the National*
625 *Academy of Sciences* **81**, 2616-2620 (1984).
- 626 93 Uemura, T. *et al.* DNA topoisomerase II is required for condensation and separation
627 of mitotic chromosomes in *S. pombe*. *Cell* **50**, 917-925 (1987).
- 628 94 Foltz, D. R. *et al.* The human CENP-A centromeric nucleosome-associated complex.
629 *Nat. Cell Biol.* **8**, 458-469 (2006).
- 630 95 Blot, J., Chartrain, I., Roghi, C., Philippe, M. & Tassan, J.-P. Cell cycle regulation of
631 pEg3, a new *Xenopus* protein kinase of the KIN1/PAR-1/MARK family. *Dev. Biol.*
632 **241**, 327-338 (2002).

- 633 96 Davezac, N., Baldin, V., Blot, J., Ducommun, B. & Tassan, J.-P. Human pEg3 kinase
634 associates with and phosphorylates CDC25B phosphatase: a potential role for pEg3 in
635 cell cycle regulation. *Oncogene* **21**, 7630-7641 (2002).
- 636 97 Badouel, C. *et al.* M-phase MELK activity is regulated by MPF and MAPK. *Cell*
637 *Cycle* **5**, 883-889 (2006).
- 638 98 Raemaekers, T. *et al.* NuSAP, a novel microtubule-associated protein involved in
639 mitotic spindle organization. *The Journal of cell biology* **162**, 1017-1029 (2003).
- 640 99 Furuse, M., Fujita, K., Hiiragi, T., Fujimoto, K. & Tsukita, S. Claudin-1 and-2: novel
641 integral membrane proteins localizing at tight junctions with no sequence similarity to
642 occludin. *The Journal of cell biology* **141**, 1539-1550 (1998).
- 643 100 Ito, K., Nakamura, H. & Watanabe, Y. Protogenin mediates cell adhesion for
644 ingression and re-epithelialization of paraxial mesodermal cells. *Dev. Biol.* **351**, 13-24
645 (2011).
- 646 101 Wong, Y.-H. *et al.* Protogenin defines a transition stage during embryonic
647 neurogenesis and prevents precocious neuronal differentiation. *J. Neurosci.* **30**, 4428-
648 4439 (2010).
- 649 102 Blaydon, D. C. *et al.* Mutations in CSTA, encoding Cystatin A, underlie exfoliative
650 ichthyosis and reveal a role for this protease inhibitor in cell-cell adhesion. *The*
651 *American Journal of Human Genetics* **89**, 564-571 (2011).
- 652 103 Kapur, R. P., Sweetser, D. A., Doggett, B., Siebert, J. R. & Palmiter, R. D.
653 Intercellular signals downstream of endothelin receptor-B mediate colonization of the
654 large intestine by enteric neuroblasts. *Development* **121**, 3787-3795 (1995).
- 655 104 Amiel, J. *et al.* Heterozygous Endothelin Receptor B (EDNRB) Mutations in Isolated
656 Hirschsprung Disease. *Hum. Mol. Genet.* **5**, 355-357 (1996).

- 657 105 Cimadamore, F., Amador-Arjona, A., Chen, C., Huang, C.-T. & Terskikh, A. V.
658 SOX2–LIN28/let-7 pathway regulates proliferation and neurogenesis in neural
659 precursors. *Proceedings of the National Academy of Sciences* **110**, E3017-E3026
660 (2013).
- 661 106 Yang, M. *et al.* Lin28 promotes the proliferative capacity of neural progenitor cells in
662 brain development. *Development* **142**, 1616-1627 (2015).
- 663 107 Robinton, D. A. *et al.* The Lin28/let-7 Pathway Regulates the Mammalian Caudal
664 Body Axis Elongation Program. *Dev. Cell* **48**, 396-405. e393 (2019).
- 665 108 Rutishauser, U., Acheson, A., Hall, A. K., Mann, D. M. & Sunshine, J. The neural cell
666 adhesion molecule (NCAM) as a regulator of cell-cell interactions. *Science* **240**, 53-
667 57 (1988).
- 668 109 Newgreen, D., Kerr, R., Minichiello, J. & Warren, N. Changes in cell adhesion and
669 extracellular matrix molecules in spontaneous spinal neural tube defects in avian
670 embryos. *Teratology* **55**, 195-207 (1997).
- 671 110 Vitureira, N. *et al.* Podocalyxin is a novel polysialylated neural adhesion protein with
672 multiple roles in neural development and synapse formation. *PLoS One* **5**, e12003
673 (2010).

674

675

676 **Acknowledgements**

677 We are grateful to Nidia De Oliveira for technical help, Claire Anderson, Jun Ong, Hyung
678 Chul Lee and Irene De Almeida for providing some probes, to Kathy Niakan, Claudia Gerri
679 and Norah Fogarty for guidance on scRNA-seq and help with the Covaris shearing (done at the
680 Francis Crick Institute, London) and to James Briscoe and Andrea Streit for helpful comments
681 on the manuscript. **Funding:** This study was funded by a Wellcome Trust 4-year PhD
682 studentship to TS (105381/Z/14/Z), a Wellcome Trust investigator award to CDS
683 (107055/Z/15/Z) and a BBSRC grant (BB/R003432/1). AM is funded by an Anatomical
684 Society studentship and NP is a Howard Hughes International Scholar and an Investigator at
685 A*STAR, Singapore.

686

687 **Author contributions**

688 H-CL processed raw RNA-seq data, AM and NP made and analysed the movie. TS performed
689 all other experiments and analysis. CDS coordinated the research and obtained the funding. TS
690 and CDS designed the project and wrote the manuscript.

691

692 **Competing interests:** Authors declare no competing interests.

693

694 **Supplementary information** is available for this paper.

695

696 **Materials and correspondence:** Correspondence and requests for materials should be
697 addressed to Claudio D. Stern, c.stern@ucl.ac.uk.

698

699 **Supplementary Information**

700

701 **Supplementary Movie**

702 **Supplementary movie 1 | Live tracking of cells in the node from HH5 to HH9.** Time-lapse

703 movie showing a mosaic of cells labelled with DsRed (pseudo-colour encoded as green).

704 Selected cells originating from the anterior part of the node at HH5 are highlighted in blue and

705 some originating from the posterior part of the node are highlighted in red. The outline of the

706 node is highlighted by a white dashed line.

707

708 **Supplementary Data**

709 **Supplementary data 1 | FPKM table for scRNA-seq data.** Transcriptional profiling of single

710 cells individually harvested from the HH8 node, originating from the three experimental

711 conditions described in Fig. 4f. Details on the epiblast origin (developmental stages and

712 position in the donor) of the cells and their positions within the host node at the time of

713 collection are included in the raw data submitted to EBI Array Express (accession number E-

714 MTAB-9116).

715

716 **Supplementary data 2 | FPKM table for bulk-RNA-seq data.** Transcriptional profiling of 6

717 sub-regions of the HH8 node (see Extended Data Fig. 7a). The raw data were submitted to EBI

718 Array Express (accession number E-MTAB-9115). Abbreviations for the node regions at stage

719 8: S15_AL8: anterior-left; S16_AR8: anterior-right; S17_ML8: middle-left; S18_MR8:

720 middle-right; S19_PL8: posterior-left; S20_PR8: posterior-right.

721